INTERNATIONAL JOURNAL FOR NUMERICAL METHODS IN FLUIDS, VOL. 19, 343–361 (1994)

BOUNDARY ELEMENT METHOD FOR STEADY 2D HIGH-REYNOLDS-NUMBER FLOW

Z. REK AND L. ŠKERGET

Faculty of Engineering, University of Maribor, Smetanova 17, SI-62000 Maribor, Slovenia

SUMMARY

This paper deals with the numerical simulation of fluid dynamics using the boundary–domain integral technique (BEM). The steady 2D diffusion–convection equations are discussed and applied to solve the plane Navier–Stokes equations. A vorticity–velocity formulation has been used. The numerical scheme was tested on the well-known 'driven cavity' problem. Results for $Re = 1000$ and 10,000 are compared with benchmark solutions. There are also results for $Re = 15{,}000$ but they have only qualitative value. The purpose was to show the stability and robustness of the method even when the grid is relatively coarse.

KEY WORDS Boundary element method Vorticity–velocity formulation Steady incompressible laminar fluid flow

1. INTRODUCTION

Very rapid advances in computing have enabled the development of numerical fluid dynamics.[1–4] Fluid dynamics is a research field full of non-linearities, strong geometrical non-regularities and singularities due to boundary conditions. The governing equations of transport phenomena are in general diffusivity–convectivity partial differential equations—the characteristics of which change strongly from point to point of the flow field owing to different local Reynolds number values—physically representing the relationship between diffusion and convection of individual parameters of state. Thus it is not possible to discriminate pure elliptic, parabolic and hyperbolic equations, since they are of mixed type.

The Navier–Stokes equations represent a system of non-linear partial differential equations of viscous Newtonian fluid motion. They provide a mathematical model of physical conservation laws of mass, energy, species and momentum for a control volume—the Eulerian case.[5] Governing equations may be written for primitive physical variables or for dependent ones. For selection of the best formulation it is of great importance which numerical technique is to be applied. There are a variety of velocity–pressure, vorticity–streamfunction, velocity–vorticity and penalty formulations, etc. available. In particular, the velocity–vorticity approach has proved successful with the boundary element method.[6,7] The advantage of the velocity–vorticity formulation lies in the numerical separation of the kinematics and kinetics of the flow from the pressure computation, which is done later by the solution of a linear system of equations for known velocity and vorticity fields.

2. NAVIER–STOKES EQUATIONS

The partial differential equation set governing the transport phenomena in steady incompressible fluid flow represents the basic conservation balances of mass and momentum, written below in

CCC 0271–2091/94/160343–19

Received April 1993
Revised March 1994

an indicial notation form for a right-handed Cartesian co-ordinate system:

$$\frac{\partial v_j}{\partial x_j} = 0, \tag{1}$$

$$\rho v_j \frac{\partial v_i}{\partial x_j} = \frac{\partial \sigma_{ij}}{\partial x_j} + \rho f_{m_i} = -\frac{\partial p}{\partial x_i} + \frac{\partial \tau_{ij}}{\partial x_j} + \rho f_{m_i}, \tag{2}$$

where v_i is the ith instantaneous velocity component, x_i is the ith co-ordinate, σ_{ij} is the stress tensor, p is the pressure, τ_{ij} is the deviatoric stress tensor, f_{m_i} stands for the body force, e.g. the gravity g_i, and ρ is the fluid mass density.

Let us obey a simple linear gradient type of constitutive hypothesis Newton law describing the relation between the stress tensor τ_{ij} and the strain tensor $\dot{\varepsilon}_{ij}$:

$$\tau_{ij} = 2\eta\dot{\varepsilon}_{ij}, \tag{3}$$

where η is the fluid dynamic viscosity.

Substituting the constitutive hypothesis equation (3) into the basic conservation law equation (2), the steady non-linear Navier–Stokes equation set can be derived, expressing the momentum transport phenomena in an incompressible Newtonian fluid flow:

$$\frac{\partial v_j}{\partial x_j} = 0, \tag{4}$$

$$v_j \frac{\partial v_i}{\partial x_j} = -\frac{1}{\rho}\frac{\partial P}{\partial x_i} + \frac{\partial}{\partial x_j}\left[\nu\left(\frac{\partial v_i}{\partial x_j} + \frac{\partial v_j}{\partial x_i}\right)\right], \tag{5}$$

where $\nu = \eta/\rho$ is the kinematic viscosity and $P = p - \rho g_j r_j$ is the modified pressure. If we assume that the material properties are constant, which is a reasonable assumption in many engineering problems, the Navier–Stokes equation set simplifies considerably and the following set of equations can be written:

$$\frac{\partial v_j}{\partial x_j} = 0, \tag{6}$$

$$\frac{\partial v_j v_i}{\partial x_j} = -\frac{1}{\rho}\frac{\partial P}{\partial x_i} + \nu\frac{\partial^2 v_i}{\partial x_j \partial x_j}. \tag{7}$$

The above equation set for constant material properties represents a closed system of equations for the determination of velocity $\vec{v}(\vec{r}, t)$ and pressure $p(\vec{r}, t)$ fields, subject to appropriate boundary conditions of velocity.

2.1. *Vorticity transport equation*

Introducing the vorticity (scalar in 2D)

$$\omega = e_{ij}\frac{\partial v_j}{\partial x_i}, \qquad e_{ij} = \begin{cases} 1, & i = 1, j = 2, \\ -1, & i = 2, j = 1, \end{cases} \tag{8}$$

the fluid motion computation scheme is partitioned into its kinematic and kinetic aspects. The kinematics is described by the continuity equation (6) and the vorticity definition (8), expressing

the relationship between the vorticity and velocity fields. The kinetics is governed by the vorticity transport equation obtained as the curl of the momentum equation (7) and describes the redistribution of the vorticity in fluid flow.

Using some basic vector identities in the convective term and taking the curl of both sides of equation (7), the steady 2D vorticity transport equation can be obtained as

$$\frac{\partial(v_j\omega)}{\partial x_j} = \nu \frac{\partial^2 \omega}{\partial x_j \partial x_j}. \tag{9}$$

The essential reason for considering the fluid motion in terms of the vorticity distribution is that the vorticity vector $\vec{\omega}$ is a solenoidal vector and so cannot be produced or destroyed in the interior of homogeneous media under normal conditions. It is produced only at the solid boundaries owing to the viscous effects. The net viscous force on an incompressible fluid particle is given by the local vorticity gradients. For a low-viscosity fluid flow the net viscous force is significant only at the point in the fluid flow of large vorticity gradients. The vorticity transport equation (9) is a highly non-linear PDE owing to the products of velocity and vorticity in the convective term and the velocity is kinematically dependent on the vorticity. Because of this inherent non- linearity, the kinetics of general viscous motion, particularly for high-Reynolds-number flows, represents a greater numerical effort than that required by the kinematics.

3. INTEGRAL REPRESENTATION OF NAVIER–STOKES EQUATIONS

The vorticity transport equation describes the development of the vorticity field in fluid flow. It is an elliptic equation representing a boundary value problem. These boundary vorticities have to be computed in the kinematics given by the elliptic equation expressing the compatibility of the velocity and vorticity fields. Since the equation represents a boundary value problem, velocity boundary conditions have to be specified. Accurate computation of the boundary vorticity values is the crucial part of the overall accuracy of the numerical scheme.

3.1. Vorticity transport equation—kinetics

Considering the spatial vorticity transfer process in integral form, one has to assume that the vorticity obeys a non-homogeneous elliptic equation[8]

$$\nu \frac{\partial^2 \omega}{\partial x_j \partial x_j} + b = 0 \quad \text{in } \Omega, \tag{10}$$

subject to the corresponding boundary conditions of the first and second kinds,

$$\begin{aligned} \omega &= \bar{\omega} \quad \text{on } \Gamma_1, \\ \frac{\partial \omega}{\partial n} &= \overline{\frac{\partial \omega}{\partial n}} \quad \text{on } \Gamma_2, \end{aligned} \tag{11}$$

while the pseudo body forces b include the convective term from equation (9),

$$b = -\frac{\partial(v_j\omega)}{\partial x_j}, \tag{12}$$

yielding the integral formulation

$$vc(\xi)\omega(\xi) + v\int_\Gamma \omega \frac{\partial u^*}{\partial n}\,d\Gamma = v\int_\Gamma \frac{\partial \omega}{\partial n} u^*\,d\Gamma - \int_\Gamma \omega v_n u^*\,d\Gamma + \int_\Omega \omega v_j \frac{\partial u^*}{\partial x_j}\,d\Omega. \tag{13}$$

Equation (13) expresses the steady 2D vorticity transport in the boundary–domain integral formulation, where $u^* = u^*(\xi, s) = (1/2\pi)\ln[r_0/r(\xi, s)]$ is the elliptic 2D fundamental solution of the equation $\nabla^2 u^*(\xi, s) + \delta(\xi, s) = 0$ which represents the influence of a unit source at point ξ on the potential field at point s. The vorticity diffusion is described by the first two boundary integrals, while the third boundary integral gives the terms representing the convective flux across the boundary, which vanishes for $v_n = 0$. The domain integral gives the influence of the transport effects in the domain due to the convection.

3.2. Vector potential equation—kinematics

The boundary–domain integral statement for the kinematics can be obtained using Green's theorem for vectors in the vector form Poisson equation for the vector potential ($\vec{v} = \vec{\nabla} \times \vec{\Psi}$),[9,10]

$$\nabla^2 \vec{\Psi} + \vec{\omega} = 0, \tag{14}$$

yielding the integral representation

$$c(\xi)\vec{v}(\xi) + \int_\Gamma (\vec{\nabla} u^* \cdot \vec{n})\vec{v}\,d\Gamma = \int_\Gamma (\vec{\nabla} u^* \times \vec{n}) \times \vec{v}\,d\Gamma + \int_\Omega \vec{\omega} \times \vec{\nabla} u^*\,d\Omega. \tag{15}$$

For the plane case where the vorticity vector $\vec{\omega}$ has only, one component ($\vec{\omega} = \omega\vec{k}$), the vector integral equation (15) represents two scalar equations for individual x and y Cartesian co-ordinate directions. The statement is completely equivalent to the continuity equation and vorticity definition, expressing the kinematics of incompressible fluid flow in integral form. Boundary velocity conditions are included in the boundary integrals, while the domain integral gives the contribution of the vorticity field to the development of the velocity field. Notice that for irrotational flow the domain integral vanishes and the kinematics of the potential fluid flow is given by the boundary integrals only. The integral equation enables the explicit computation of the velocity components in the interior of the domain. Boundary vorticity values are also given in integral form within the domain integral, thus eliminating the need to use some approximate formula based on Taylor series expansion for determining the vorticity on the boundary, which would introduce additional error into the numerical scheme employed. The computation of the boundary vorticities in the frame of classical domain-type numerical techniques, i.e. finite elements and finite differences, is the most critical part of the numerical scheme, since it controls the overall quality of the numerical solution.

When the unknowns are the boundary vorticity values or the tangential velocity components to the boundary, one has to use the tangential form of the vector equation (15), i.e.

$$c(\xi)\vec{n}(\xi) \times \vec{v}(\xi) + \vec{n}(\xi) \times \int_\Gamma (\vec{\nabla} u^* \cdot \vec{n})\vec{v}\,d\Gamma = \vec{n}(\xi) \times \int_\Gamma (\vec{\nabla} u^* \times \vec{n}) \times \vec{v}\,d\Gamma + \vec{n}(\xi) \times \int_\Omega \vec{\omega} \times \vec{\nabla} u^*\,d\Omega, \tag{16}$$

or when the normal velocity components to the boundary are unknown, the normal form of the equation has to be employed, i.e.

$$c(\xi)\vec{n}(\xi)\cdot\vec{v}(\xi)+\vec{n}(\xi)\cdot\int_\Gamma(\vec{\nabla}u^*\cdot\vec{n})\vec{v}\,d\Gamma=\vec{n}(\xi)\cdot\int_\Gamma(\vec{\nabla}u^*\times\vec{n})\times\vec{v}\,d\Gamma+\vec{n}(\xi)\cdot\int_\Omega\vec{\omega}\times\vec{\nabla}u^*\,d\Omega, \quad (17)$$

in order to obtain the appropriate non-singular implicit system of equations.

4. NUMERICAL SOLUTION—KINETICS

For the numerical solution of the kinetic equation the corresponding boundary–domain integral representation is written in a discretized form in which the integrals over the boundary and domain are approximated by a summation of integrals over individual boundary elements or internal cells respectively, e.g. in the general discretized representation of the integral equation (13),[11–14]

$$c(\xi)\omega(\xi)+\sum_{e=1}^{N_E}\int_{\Gamma_e}\omega\frac{\partial u^*}{\partial n}\,d\Gamma=\sum_{e=1}^{N_E}\int_{\Gamma_e}\frac{\partial\omega}{\partial n}u^*\,d\Gamma-\frac{1}{\nu}\sum_{e=1}^{N_E}\int_{\Gamma_e}\omega v_n u^*\,d\Gamma+\frac{1}{\nu}\sum_{c=1}^{N_C}\int_{\Omega_c}\omega v_j\frac{\partial u^*}{\partial x_j}\,d\Omega, \quad (18)$$

where N_E boundary elements and N_C internal cells are employed. Next the variation in all field functions or the products of field functions within each boundary element or internal cell is approximated by the use of interpolation polynomials $\{\Phi\}$ and $\{\varphi\}$ with respect to boundary or domain and nodal function values. Let the index n refer to the number of nodes in each boundary element or internal cell and also relate to the degree of the respective interpolation polynomials. It should be mentioned that the degree of interpolation polynomials on the boundary elements and in internal cells can differ.

To solve equation (18), the implicit system of equations is written simultaneously for all boundary and internal points, resulting in a very large, fully populated system matrix which is influenced by diffusion and convection. The consequence of this fact is that the numerical scheme is very stable and accurate regardless of the Reynolds number values.

The discretized form of the integral equation (18) can thus be written as

$$c(\xi)\omega(\xi)+\sum_{e=1}^{N_E}\{h\}^T\{\omega\}^n=\sum_{e=1}^{N_E}\{g\}^T\left\{\frac{\partial\omega}{\partial n}\right\}^n-\frac{1}{\nu}\sum_{e=1}^{N_E}\{g\}^T[v_n]\{\omega\}^n+\frac{1}{\nu}\sum_{c=1}^{N_C}\{d_j\}^T[v_j]\{\omega\}^n, \quad (19)$$

where h, g and d_j represent integrals over boundary elements and internal cells respectively. Applying equation (19) to all boundary and internal nodes $\xi=1,\ldots,m$, the matrix equation

$$\left([H]+\frac{1}{\nu}[G][v_n]-\frac{1}{\nu}[D_j][v_j]\right)\{\omega\}=-\frac{1}{\nu}[G]\{q\},\qquad \{q\}=-\nu\left\{\frac{\partial\omega}{\partial n}\right\} \quad (20)$$

is obtained when the vorticity is unknown (q is the diffusion flux), or

$$\left([H]-\frac{1}{\nu}[D_j][v_j]\right)\{\omega\}=-\frac{1}{\nu}[G]\{q\},\qquad \{q\}=-\nu\left\{\frac{\partial\omega}{\partial n}\right\}+\frac{1}{\nu}[v_n]\{\omega\} \quad (21)$$

when the vorticity flux is unknown (q is the total flux = diffusion + convection). In symbolic matrix notation of an implicit non-linear system of m equations for all boundary and domain unknown values one can write

$$[E]\{\omega\}^{k+1} = -\frac{1}{\nu}[G]\{q\}^{k+1}, \tag{22}$$

where k stands for the iterative step. Accounting for the boundary conditions, e.g. known nodal vorticity values $\{\omega\}$ on Γ_1 and vorticity flux values $\{\partial\omega/\partial n\}$ on Γ_2 ($\Gamma = \Gamma_1 + \Gamma_2$), equation (22) can be reordered as

$$[A]\{X\}^{k+1} = \{F_0\}. \tag{23}$$

The system matrix $[A]$ is composed of the influence matrices $[G]$ and $[E]$, $\{X\}$ is the vector of unknowns and $\{F_0\}$ is the right-hand-side term.

Notice that the matrix $[E]$ in equation (22) and the system matrix $[A]$ in equation (23) are influenced by the velocity field and as such they have to be computed again at each particular iterative step. Since the order of the matrix $[A]$ is very large and equal to the number of all boundary and internal points, it is desirable to avoid performing the triangularization step in the Gauss solution algorithm at each iterative step. This can be accomplished by partitioning the velocity field into known and unknown variable parts, e.g. $\{v_j\} = \{\bar{v}_j\} + \{\tilde{v}_j\}$, yielding from equation (20) the matrix statement

$$[A]\{X\}^{k+1} = \{F_0\} + \{F_N(\tilde{v}_j, u)\}^k. \tag{24}$$

The system matrix $[A]$ is now based on the known velocity field part $\{\bar{v}_j\}$ only and can be kept constant for several iterative steps. The influence of the variable velocity field part $\{\tilde{v}_j\}$ is included in the non-linear right-hand-side vector $\{F_N\}$, i.e.

$$\{F_N\} = -\frac{1}{\nu}([G](\tilde{v}_n] - [D_j][\tilde{v}_j])\{\omega\}. \tag{25}$$

5. NUMERICAL SOLUTION—KINEMATICS

For the numerical solution of the kinematic equation (15) the corresponding discretized form with analogy to the kinetics can be written as[6,7,15]

$$\begin{aligned} c(\xi)v_x(\xi) + \sum_{e=1}^{N_E}\{h\}^T\{v_x\}^n &= \sum_{e=1}^{N_E}\{h_t\}^T\{v_y\}^n - \sum_{c=1}^{N_C}\{d_y\}^T\{\omega\}^n, \\ c(\xi)v_y(\xi) + \sum_{e=1}^{N_E}\{h\}^T\{v_y\}^n &= -\sum_{e=1}^{N_E}\{h_t\}^T\{v_x\}^n + \sum_{c=1}^{N_C}\{d_x\}^T\{\omega\}^n, \end{aligned} \tag{26}$$

where an additional integral h_t appears. Applying equations (26) to all boundary nodes, the following $2N_E$ matrix systems are obtained:

$$\begin{aligned} [c(\xi)]\{v_x(\xi)\} + [\hat{H}]\{v_x\} &= [H_t]\{v_y\} - [D_y]\{\omega\}, \\ [c(\xi)]\{v_y(\xi)\} + [\hat{H}]\{v_y\} &= -[H_t]\{v_x\} + [D_x]\{\omega\}, \end{aligned} \tag{27}$$

A system of N_E equations for N_E unknown boundary values can be readily derived by multiplying

the above two systems of equations by the unit tangent when the boundary vorticity or tangential velocity component is unknown, according to equation (16), i.e.

$$[E_t]\{v_n\} = [F_n]\{v_t\} + [D_n]\{\omega\}, \tag{28}$$

and by multiplying by the unit normal when the normal velocity component is unknown, according to equation (17), i.e.

$$[E_n]\{v_n\} = [F_t]\{v_t\} + [D_t]\{\omega\}. \tag{29}$$

The velocity components in the domain are then obtained explicitly for $c(\xi) = 1$ as

$$\begin{aligned} \{v_x(\xi)\} &= -[\hat{H}]\{v_x\} + [H_t]\{v_y\} - [D_y]\{\omega\}, \\ \{v_y(\xi)\} &= [\hat{H}]\{v_y\} - [H_t]\{v_x\} + [D_x]\{\omega\}. \end{aligned} \tag{30}$$

6. BOUNDARY CONDITIONS AND SOLUTION PROCEDURE

The boundary conditions have a great influence on the behaviour of the numerical scheme. If they do not match the physics of the problem, the numerical scheme will not converge.

The most natural and simplest boundary conditions arise when the velocity is known over all the boundary. In this case only the boundary vorticity values are unknown in the set of kinematic equations, assuming some initial values for the vorticity in the domain. The velocity field in the domain is then obtained by an explicit computation from the known vorticity field and prescribed boundary velocity values. The only unknowns which appear in the kinetic system of equations are therefore the vorticity flux and the domain vorticity and these can be easily obtained.

More difficulties arise when the velocity is not known *a priori* over part of the boundary (outflow region). In such a case a reasonable choice is to assume zero vorticity flux through the boundary and zero tangential component of the velocity. The unknowns which appear in the kinematics are therefore the boundary vorticity (where the velocity is prescribed) and the normal component of the velocity (where the vorticity flux is prescribed). In the kinetic part the unknowns are the vorticity flux (where the velocity is prescribed), the boundary vorticity (where the vorticity flux is prescribed) and the domain vorticity.

A third type of boundary condition appears when symmetry is prescribed over part of the boundary. In this case the vorticity and the normal component of the velocity are zero. The unknowns that appear in the kinematic system are the boundary vorticity (where the velocity is prescribed) and the tangential component of the velocity (where the normal component is prescribed). In the kinetic part the unknowns are the vorticity flux (on all the boundary) and the domain vorticity.

The kinematic relations and vorticity kinetic equation are coupled in a set of non-linear equations. An iterative point underrelaxation solution procedure has to be employed. The underrelaxation factor r depends on the Reynolds number and the mesh (a finer mesh implies a smaller value of r). To get a solution of the problem, one has to perform the following steps:

1. Start with some initial values for vorticity.
2. Kinematic part.
   (a) First type of BC— solve system for boundary values for vorticity.
   (b) Second type of BC—solve system for boundary values for vorticity and normal component of velocity.

(c) Third type of BC—solve system for boundary values for vorticity and tangential component of velocity.

Calculate domain velocity components in an explicit manner.

3. Kinetic part.
   (a) First type of BC—solve system of equations for unknown boundary vorticity fluxes and domain vorticity values.
   (b) Second type of BC—solve system of equations for unknown boundary vorticity, vorticity fluxes and domain vorticity.
   (c) Third type of BC—solve system of equations for unknown boundary vorticity fluxes and domain vorticity values.
4. Relax vorticity values and check convergence. If convergence criterion is satisfied, then stop; otherwise go to step 2.

7. TEST CASE

The described BEM scheme has been tested on a standard test case to evaluate the numerical scheme. The test case is the well-known 'driven cavity flow' and it is used because there have been a lot of results obtained by other authors using different numerical approaches. As a benchmark solution of the problem, with which our results are compared, the work of Ghia *et al.*[16] has been used.

7.1. Discrete model

The problem consists of a square cavity totally filled with an incompressible viscous fluid and a top wall moving with constant velocity. The geometry and boundary conditions are shown in Figure 1. In the discretized model, 160 mixed-type boundary elements are used with linear interpolation for the vorticity and constant interpolation for the vorticity flux. The reason for using a discontinuous approximation for the flux is the singularity of the corners, where the normal vector is not defined. Such a choice is also physically reasonable, because the vorticity

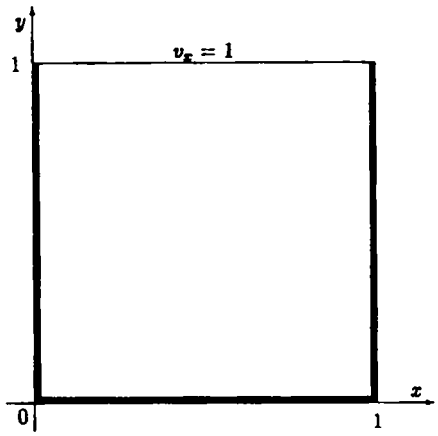

Figure 1. Geometry and boundary conditions

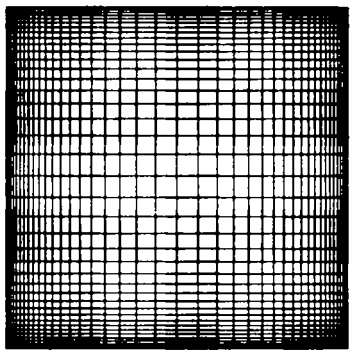

Figure 2. Discretized model

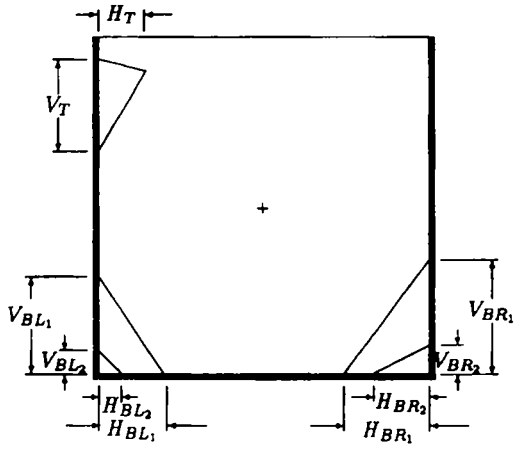

Figure 3. Cavity flow nomenclature

is continuous over the boundary but the vorticity flux can be different at corner points. For domain discretization, 1600 cells with bilinear interpolation have been used. There are 41 × 41 nodes, which gives us a total of 1681 unknowns. The mesh was non-uniform, with ratio of 10 between the largest and the smallest boundary element, and symmetric with respect to the centre of the cavity (Figure 2).

Three cases were studied in this analysis: $Re = 1000$, 10,000 and 15,000. Owing to the movement of the top wall, a large vortex appears in the central region and also small vortices at the corners. The primary vortex with its centre near the geometric centre of the cavity always appears, while the number, length and position of secondary vortices depend on Re. The nomenclature is given in Figure 3.

7.2. *Results*

The results of the analysis agree well with the benchmark solution, bearing in mind that the mesh density was 41 × 41 nodes while in the benchmark case there were 129 × 129 nodes for $Re = 1000$ and 257 × 257 nodes for $Re = 10{,}000$. The iteration process was stopped when

the residual error (square root of the residual vector for the kinetic equation) became less than 1% of the initial error; 160 iterations were needed at $Re = 1000$ and 240 iterations at $Re = 10{,}000$ to reach this error. However, for $Re = 15{,}000$ only 10% residual error had been reached after 400 iterations. Owing to the very strong non-linearity which appears at high Re, a very small underrelaxation factor has to be used, such as $r = 0{\cdot}01$ and $r = 0{\cdot}001$ for $Re = 1000$, 10,000 and $Re = 15{,}000$ respectively.

Table I. Velocity v_x along vertical line through centre of cavity

	$Re = 1000$		$Re = 10{,}000$	
y	BEM	Benchmark	BEM	Benchmark
1·0000	1·00000	1·00000	1·00000	1·00000
0·9766	0·66420	0·65928	0·42800	0·47221
0·9688	0·57798	0·57492	0·43131	0·47783
0·9609	0·51229	0·51117	0·44079	0·48070
0·9531	0·46731	0·46604	0·44142	0·47804
0·8516	0·32704	0·33304	0·31847	0·34635
0·7344	0·18460	0·18719	0·19070	0·20673
0·6172	0·05620	0·05702	0·08128	0·08344
0·5000	−0·05919	−0·06080	−0·02155	−0·03111
0·4531	−0·10376	−0·10648	−0·06258	−0·07540
0·2813	−0·27357	−0·27805	−0·20715	−0·23186
0·1719	−0·36186	−0·38289	−0·30193	−0·32709
0·1016	−0·27803	−0·29730	−0·35927	−0·38000
0·0703	−0·20955	−0·22220	−0·40219	−0·41657
0·0625	−0·19108	−0·20196	−0·40450	−0·42537
0·0547	−0·17187	−0·18109	−0·39788	−0·42735
0·0000	0·00000	0·00000	0·00000	0·00000

Table II. Velocity v_y along horizontal line through centre of cavity

	$Re = 1000$		$Re = 10{,}000$	
x	BEM	Benchmark	BEM	Benchmark
1·0000	1·00000	1·00000	1·00000	1·00000
0·9688	−0·19914	−0·21388	−0·50722	−0·54302
0·9609	−0·25653	−0·27669	−0·50150	−0·52987
0·9531	−0·31002	−0·33714	−0·46465	−0·49099
0·9453	−0·35944	−0·39188	−0·42775	−0·45863
0·9063	−0·48628	−0·51550	−0·40072	−0·41496
0·8594	−0·41692	−0·42665	−0·32615	−0·36737
0·8047	−0·31024	−0·31966	−0·28221	−0·30719
0·5000	0·01846	0·02526	0·01103	0·00831
0·2344	0·30357	0·32235	0·24697	0·27224
0·2266	0·31216	0·33075	0·25421	0·28003
0·1563	0·36118	0·37095	0·32151	0·35070
0·0938	0·33356	0·32627	0·38697	0·41487
0·0781	0·31399	0·30353	0·40385	0·43124
0·0703	0·30109	0·29012	0·40576	0·43733
0·0625	0·28672	0·27485	0·40405	0·43983
0·0000	0·00000	0·00000	0·00000	0·00000

Table III. Vorticity along moving boundary

	$Re = 1000$		$Re = 10{,}000$	
x	BEM	Benchmark	BEM	Benchmark
0·0000	—	—	—	—
0·0625	62·23349	75·59800	124·55856	209·45200
0·1250	45·85837	51·05570	103·25241	145·07300
0·1875	37·64014	40·54370	93·65113	127·92800
0·2500	30·74528	32·29530	87·49921	116·27500
0·3125	24·78911	25·43410	74·92119	90·02310
0·3750	20·07527	20·26660	61·08301	67·14000
0·4375	16·83105	16·83500	46·61375	53·59050
0·5000	14·97980	14·89010	46·08840	46·82710
0·5625	14·19961	14·09280	38·50391	44·32870
0·6250	14·21242	14·13740	43·22482	44·63030
0·6975	14·76828	14·80610	43·31565	46·85720
0·7500	15·80225	16·04580	44·75240	50·37920
0·8125	17·85182	18·31200	48·69596	54·37250
0·8750	23·29794	23·87070	53·20258	57·77560
0·9375	40·95456	43·11240	61·13929	66·03520
1·0000	—	—	—	—

Tables I and II give the results for the velocity v_x and v_y profiles through the geometric centre of the cavity respectively, while in Table III the vorticity values along the moving boundary are given. One can see in the tables that the BEM results are compared with the benchmark results, but it has to be mentioned that the BEM values are obtained by an interpolation procedure, because the numbers of BEM and benchmark nodes do not coincide owing to the different meshes used.

There are large differences between the BEM and benchmark values for the vorticity along the moving boundary in Table III. The reasons for this discrepancy are as follows.

1. The mesh near the wall is much denser in the benchmark case than in the BEM, so the gradients of the velocity in the former case are better described. This can also be seen in the velocity profiles, where the differences are small away from the wall but larger close to the wall.
2. One can see that the differences increase towards the corners. This occurs because the normal to the boundary cannot be properly defined, so some average value for the unit normal is used for computation of the normal component of the velocity in the kinematic equation. This source of error can be reduced by mesh refinement near the corners.

The BEM numerical results for $Re = 15{,}000$ are not presented, because the grid was too sparse to appropriately describe the boundary layer. The results have only qualitative value and show that the numerical scheme is stable even when the discretized model is not adequate.

Values for the streamline and vorticity contours which are used in the figures are presented in Table IV. It has to be noted that the streamline values are obtained when post-processing is performed on a known velocity field, because the $\vec{v}$–$\vec{\omega}$ formulation is used, as against the benchmark solution with the $\vec{\psi}$–$\vec{\omega}$ approach; thus the comparison for streamlines has to take this fact into account.

Figure 4 presents velocity v_x profiles along the vertical and Figure 5 velocity v_y profiles along

Table IV. Values for streamline and vorticity contours in figures

Contour letter	Value of ψ	Value of ω
A	$-1{\cdot}0 \times 10^{-10}$	0·0
B	$-1{\cdot}0 \times 10^{-7}$	±0·5
C	$-1{\cdot}0 \times 10^{-5}$	±1·0
D	$-1{\cdot}0 \times 10^{-4}$	±2·0
E	−0·0100	±3·0
F	−0·0300	±4·0
G	−0·0500	±5·0
H	−0·0700	
I	−0·0900	
J	−0·1000	
K	−0·1100	
L	−0·1150	
M	−0·1175	
N	$1{\cdot}0 \times 10^{-8}$	
O	$1{\cdot}0 \times 10^{-7}$	
P	$1{\cdot}0 \times 10^{-6}$	
Q	$1{\cdot}0 \times 10^{-5}$	
R	$5{\cdot}0 \times 10^{-5}$	
S	$1{\cdot}0 \times 10^{-4}$	
T	$2{\cdot}5 \times 10^{-4}$	
U	$5{\cdot}0 \times 10^{-4}$	
V	$1{\cdot}0 \times 10^{-3}$	
W	$1{\cdot}5 \times 10^{-3}$	
X	$3{\cdot}0 \times 10^{-3}$	

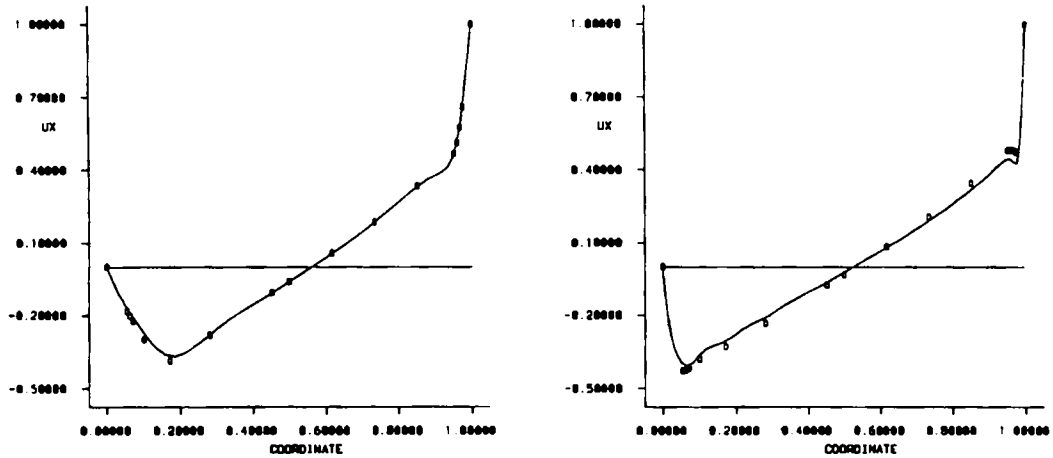

$Re = 1\,000$ $Re = 10\,000$

Figure 4. Comparison of velocity v_x along vertical line through geometric centre (———, BEM; ○, benchmark)

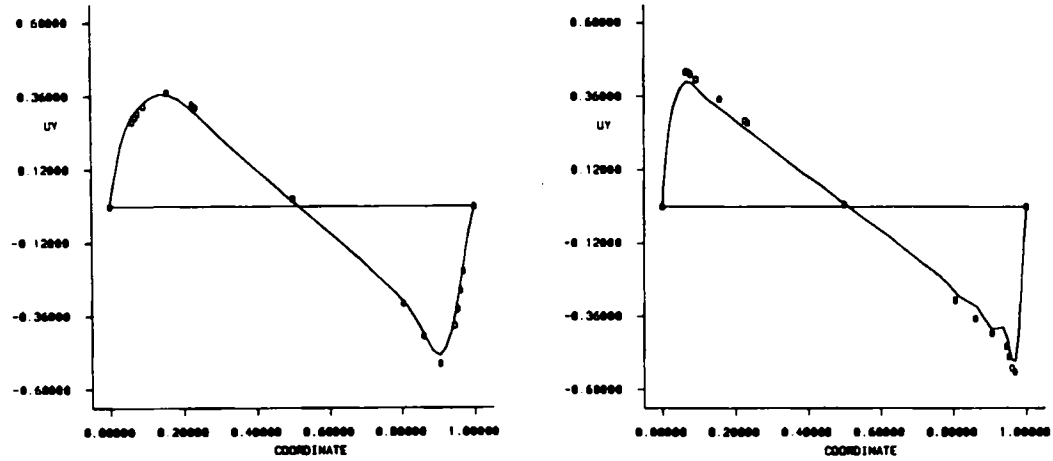

$Re = 1\,000$ $Re = 10\,000$

Figure 5. Comparison of velocity v_y along horizontal line through geometric centre (———, BEM; ○, benchmark)

the horizontal through the geometric centre of the cavity. Benchmark results are superimposed on the BEM solution. Streamline plots are presented in Figure 6, vorticity contours in Figure 7, velocity fields in Figure 8 and vorticity surfaces in Figure 9.

Properties of vortices for $Re = 1000$ and 10,000 are presented in Table V and compared with those of the benchmark solution. It can be seen that the mesh of 41 × 41 nodes is too coarse for the appearance of second vortices at the bottom corners, while the results for primary and first secondary vortices compare quite well with the benchmark solution.

8. CONCLUSION

The boundary element method is applied to the numerical simulation of incompressible viscous fluid flow. The vorticity–velocity formulation is used to solve the fluid motion problem. Introducing the vorticity, the computation of the problem is partitioned into its kinematics and kinetics parts. The behaviour and physical meanings of the different terms in the integral equations are discussed. Owing to the fundamental solution, a part of the transport mechanism is transferred to the boundary, producing a very stable numerical scheme. Different degrees of interpolation for a function and its normal derivative were used to avoid problems with corners, where the normal to the boundary is not defined. Comparison of the BEM results with the benchmark solution shows good agreement, bearing in mind the relatively coarse grid.

The weakness of the presented method is that the matrices are fully populated, not diagonally dominant and non-positive definite, so that special solvers cannot be used. The consequence of this is a very long computation time compared with other methods. This means that the described scheme in its present form is not applicable for problems where very fine discretization is required. However, BEM is a relatively new method and is developing fast.

Extensive work on the 'subdomain technique' and the use of iterative solvers is currently in progress.[17,18] The influence of other types of Green functions on the stability of the numerical scheme is also being studied.[19,20] We believe that such an improved BEM will be competitive with other numerical methods in real applications.

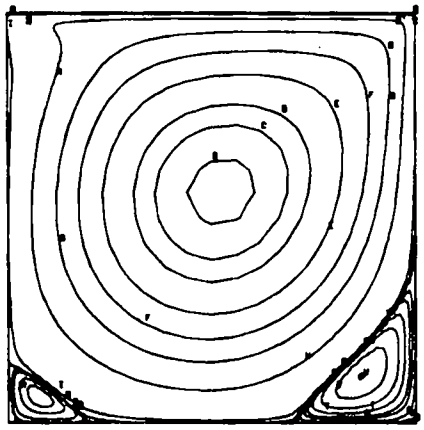

$Re = 1\,000$

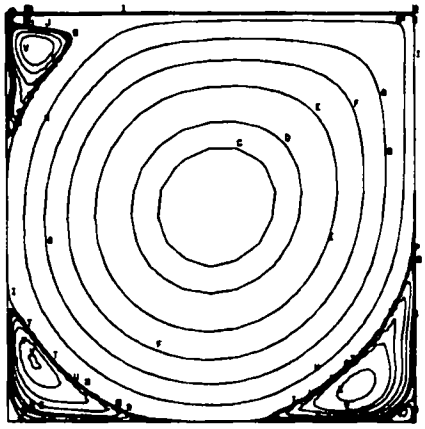

$Re = 10\,000$

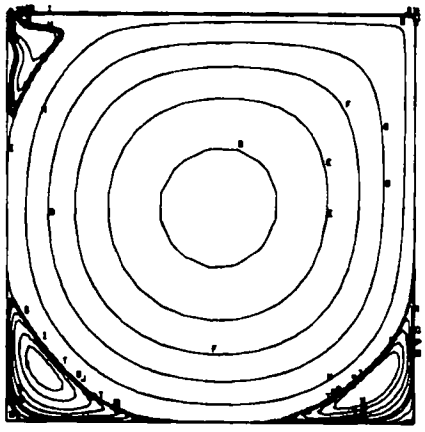

$Re = 15\,000$

Figure 6. Streamline patterns for primary and secondary vortices

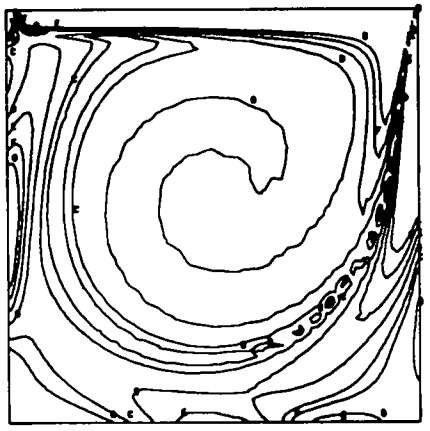

$Re = 1\,000$

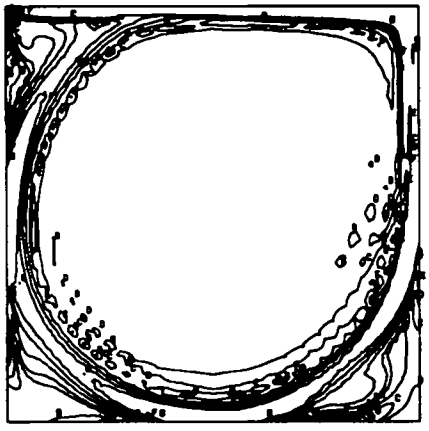

$Re = 10\,000$

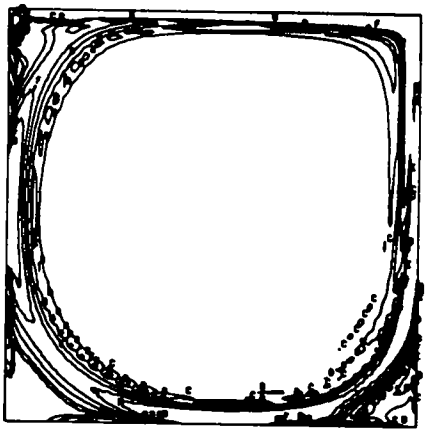

$Re = 15\,000$

Figure 7. Vorticity contours for flow in driven cavity

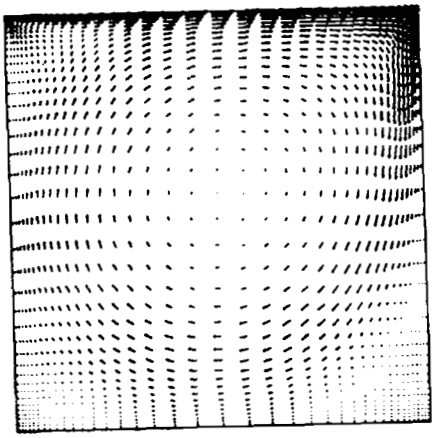

$Re = 1\,000$

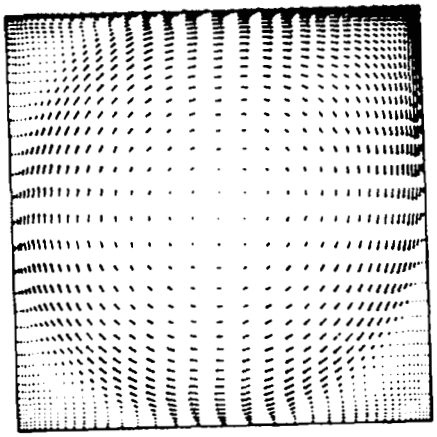

$Re = 10\,000$

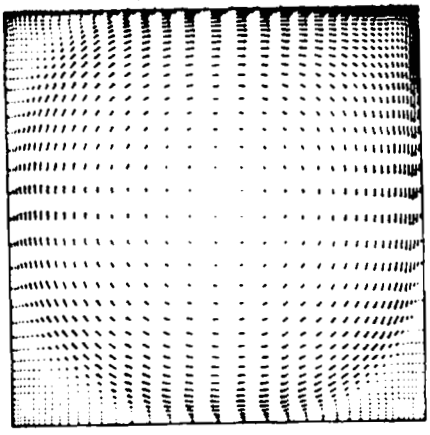

$Re = 15\,000$

Figure 8. Velocity field for flow in driven cavity

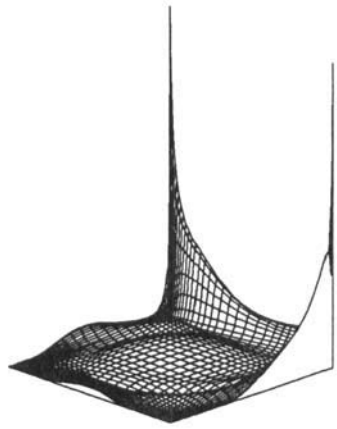

$Re = 1\,000$

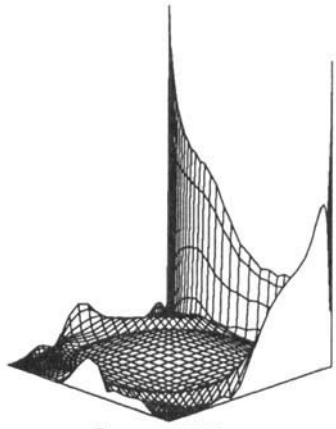

$Re = 10\,000$

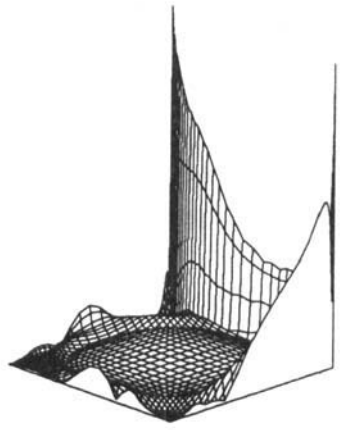

$Re = 15\,000$

Figure 9. Vorticity surfaces for flow in driven cavity

Table V. Properties of primary and secondary vorticies

Vortex	Property	Re = 1000		Re = 10,000	
		BEM	Benchmark	BEM	Benchmark
Primary	ψ_{min}	−0·113	−0·118	−0·109	−0·119
	ω_{vc}	1·977	2·049	1·784	1·881
	@x, y	0·524, 0·565	0·531, 0·562	0·514, 0·526	0·512, 0·533
First T	ψ_{max}	—	—	$2{\cdot}136 \times 10^{-3}$	$2{\cdot}421 \times 10^{-3}$
	ω_{vc}	—	—	−1·863	−2·183
	@x, y	—	—	0·079, 0·904	0·070, 0·914
	H_L	—	—	0·159	0·159
	V_L	—	—	0·311	0·320
First BL	ψ_{max}	$1{\cdot}406 \times 10^{-4}$	$2{\cdot}311 \times 10^{-4}$	$1{\cdot}558 \times 10^{-3}$	$1{\cdot}518 \times 10^{-3}$
	ω_{vc}	−0·283	−0·361	−2·161	−2·085
	@x, y	0·079, 0·065	0·086, 0·078	0·065, 0·159	0·058, 0·164
	H_L	0·216	0·219	0·382	0·344
	V_L	0·136	0·168	0·289	0·289
First BR	ψ_{max}	$1{\cdot}538 \times 10^{-3}$	$1{\cdot}751 \times 10^{-3}$	$3{\cdot}758 \times 10^{-3}$	$3{\cdot}418 \times 10^{-3}$
	ω_{vc}	−1·023	−1·155	−2·526	−4·053
	@x, y	0·854, 0·115	0·859, 0·109	0·864, 0·079	0·765, 0·058
	H_L	0·289	0·303	0·382	0·391
	V_L	0·437	0·3536	0·438	0·449
Second BL	ψ_{min}	—	—	—	$-7{\cdot}756 \times 10^{-7}$
	ω_{vc}	—	—	—	$2{\cdot}754 \times 10^{-2}$
	@x, y	—	—	—	0·015, 0·019
	H_L	—	—	—	0·035
	V_L	—	—	—	0·044
Second BR	ψ_{min}	—	$-9{\cdot}319 \times 10^{-8}$	$-1{\cdot}411 \times 10^{-5}$	$-1{\cdot}313 \times 10^{-4}$
	ω_{vc}	—	$8{\cdot}528 \times 10^{-3}$	0·189	$3{\cdot}125 \times 10^{-1}$
	@x, y	—	0·992, 0·008	0·970, 0·021	0·933, 0·062
	H_L	—	0·008	0·115	0·170
	V_L	—	0·008	0·115	0·137

ACKNOWLEDGEMENT

The authors wish to thank the Computing Centre of the Institute Jožef Stefan in Ljubljana, which enabled the case evaluation on the Convex C220 computer.

REFERENCES

1. A. J. Backer, *Finite Element Computational Fluid Mechanics*, Hemisphere, New York, 1983.
2. P. J. Roache, *Computational Fluid Dynamics*, Hermosa, Albuquerque, NM, 1982.
3. C. Taylor and T. G. Hughes, *Finite Element Programming of the Navier–Stokes Equations*, Pineridge, Swansea, 1981.
4. F. Thomasset, *Implementation of Finite Element Methods for Navier–Stokes Equations*, Springer, New York, 1981.
5. G. K. Batchelor, *An Introduction to Fluid Dynamics*, Cambridge University Press, Cambridge, 1967.
6. P. Skerget, A. Alujevic, C. A. Brebbia and G. Kuhn, 'Natural and forced convection simulation using the velocity–vorticity approach', *Topics in Boundary Element Research*, Vol. 5, Springer, Berlin, 1989, Chap. 4, pp. 49–86.
7. J. C. Wu, 'Problems of general viscous flow', in *Developments in BEM*, Vol. 2, Elsevier, London, 1982, Chap. 2.
8. P. Skerget and C. A. Brebbia, 'The solution of convective problems in laminar flow, *Proc. 5th Int. Conf. on BEM*, Springer, Berlin, 1983.

9. J. C. Wu and J. F. Thompson, 'Numerical solution of time dependent incompressible Navier–Stokes equations using an integro-differential formulation', *Comput. Fluids*, 1, 197–215 (1973).
10. P. Skerget, A. Alujevic, G. Kuhn and C. A. Brebbia, 'Natural convection flow problems by BEM', *Proc. 9th Int. Conf. on BEM*, Springer, Berlin, 1987, pp. 401–418.
11. C. A. Brebbia, *The Boundary Element Method for Engineers*, Pentech, London/Halstead, New York, 1978.
12. C. A. Brebbia, J. C. F. Telles and L. C. Wrobel, *Boundary Element Methods—Theory and Applications*, Springer, New York, 1984.
13. Z. Rek, P. Skerget and A. Alujevic, 'Boundary–domain integral method for mixed convection', *Proc. Int. Conf. on Boundary Element Methods*, Vol. 2, 1990, pp. 219–230.
14. P. Skerget, A. Alujevic, I. Zagar, Z. Rek, M. Hribersek and M. Delic, 'Boundary element method for fluid dynamics', *Proc. Boundary Elements XIV Conf.*, Springer, Berlin, 1992, pp. 73–104.
15. Z. Rek, P. Skerget and A. Alujevic, 'Vorticity–velocity formulation for turbulent flow by BEM', in *Boundary Elements in Fluid Dynamics*, Computational Mechanics Publications, Southampton, 1992, pp. 123–130.
16. U. Ghia, K. N. Ghia and C. T. Shin, 'High-*Re* solutions for incompressible flow using the Navier–Stokes equations and a multigrid method', *J. Comput. Phys.*, **48**, 387–411 (1982).
17. M. Hriberšek, L. Škerget and I. Žagar, 'Boundary–domain integral method with subdomain technique for time dependent viscous flow analysis', *ZAMM*, 73, T935–T939 (1993).
18. M. Hriberšek and L. Škerget, 'Preconditioned iterative methods for boundary domain integral method', in *Numerical Methods in Laminar and Turbulent Flow*, Vol. VIII, Part 2, Pineridge, Swansea, 1993, pp. 1541–1551.
19. I. Žagar, L. Škerget and A. Alujevič, 'Green's function in fluid dynamics', in *Numerical Methods in Laminar and Turbulent Flow*, Vol. VIII, Part 2, Pineridge, Swansea, 1993, pp. 1622–1533.
20. I. Žagar and L. Škerget, 'Stability investigations of the combined boundary–domain integral formulation', *ZAMM*, 73, T928–T931 (1993).